HHS Public Access

Author manuscript

Dev Dyn. Author manuscript; available in PMC 2020 April 24.

Published in final edited form as:

Dev Dyn. 2020 February ; 249(2): 245–261. doi:10.1002/dvdy.130.

Zebrafish *etv2* knock-in line labels vascular endothelial and blood progenitor cells

Brendan Chestnut[1], **Saulius Sumanas**[1,2,*]

[1]Division of Developmental Biology, Cincinnati Children's Hospital Medical Center, Cincinnati, OH 45229, USA

[2]Department of Pediatrics, University of Cincinnati College of Medicine, Cincinnati, OH 45229, USA

Abstract

Background: ETS transcription factor Etv2 / Etsrp is one of the earliest markers for vascular and hematopoietic progenitors and functions as a key regulator of hematovascular development in multiple vertebrates, including zebrafish. Therefore transgenic *etv2* reporter lines provide a valuable tool to study vasculogenesis and hematopoiesis. However, previously generated zebrafish reporter lines do not fully recapitulate the endogenous pattern of *etv2* expression.

Results: Here we used CRISPR / Cas9-mediated homology-independent DNA repair approach to knock-in a Gal4 transcriptional activator into the zebrafish *etv2* genomic locus, thus generating $etv2^{ci32Gt}$ gene trap line. $etv2^{ci32Gt}$*; UAS:GFP* embryos show GFP expression in vascular endothelial, myeloid and red blood cells. Because *gal4* insertion interrupts the *etv2* locus, homozygous $etv2^{ci32Gt}$ embryos display defects in vasculogenesis and myelopoiesis, and enable visualizing *etv2*-deficient hematovascular progenitors in live embryos. Furthermore, we performed differential transcriptome analysis of sorted GFP-positive cells from heterozygous and homozygous $etv2^{ci32Gt}$ embryos. Approximately 500 downregulated genes were identified in $etv2^{ci32Gt}$ homozygous embryos, which include multiple genes expressed in vascular endothelial and myeloid cells.

Conclusions: The $etv2^{ci32Gt}$ gene trap line and the datasets of misregulated genes will be valuable resources to study hematopoietic and vascular development.

Keywords

CRISPR; Cas9; RNA-seq; transcriptome; vascular endothelial; myeloid; red blood cell; zebrafish

INTRODUCTION

During vertebrate embryogenesis, vascular endothelial progenitors originate in the yolk sac and / or lateral plate mesoderm and coalesce into the first embryonic blood vessels. An evolutionarily conserved ETS transcription factor Etv2 / ER71/ Etsrp is one of the earliest

*Corresponding author. Address: Division of Developmental Biology, Cincinnati Children's Hospital Medical Center, 3333 Burnet Ave, Cincinnati, OH 45229, USA. saulius.sumanas@cchmc.org.

markers of vascular endothelial and hematopoietic progenitors (Sumanas and Lin, 2006; Pham et al., 2007; Lee et al., 2008; Sumanas et al., 2008). In zebrafish, an advantageous model system to study early hematovascular development, *etv2* is expressed in all vascular endothelial progenitors which originate in the anterior and posterior lateral plate mesoderm (ALPM or PLPM, respectively) (Sumanas and Lin, 2006; Sumanas et al., 2008). Zebrafish *etv2* mutants and morpholino knockdown embryos display nearly complete loss of early vascular endothelial differentiation prior to 24 hpf (Sumanas and Lin, 2006). At later developmental stages, vascular development partially recovers due to the redundancy of *etv2* with a related ETS transcription factor *fli1b* (Craig et al., 2015). In addition to its role in vascular development, *etv2* is also required for myelopoiesis in zebrafish embryos (Sumanas et al., 2008). Etv2 MO-injected zebrafish embryos display loss of myeloid cells, suggesting that *etv2* functions in early myeloid progenitors which originate in the zebrafish ALPM region. These *etv2* functions are conserved between vertebrate embryos, and mouse *Etv2* mutant embryos show failure of yolk sac and intraembryonic vasculogenesis and hematopoiesis (Lee et al., 2008; Ferdous et al., 2009).

Because *etv2* is one of the earliest markers for hematopoietic and vascular progenitors, *etv2* transgenic reporter lines have been a valuable tool to study vascular and hematopoietic development. A few such zebrafish reporter lines have been previously generated and include the *TgBAC(etv2:GFP)*, which was generated by BAC recombineering (Proulx et al., 2010), and the *Tg(−2.3 etv2:GFP)* reporter line, which contains 2.3 kb region of the *etv2* promoter and the first intron (Veldman and Lin, 2012). Both of these lines appear to recapitulate *etv2* expression in vascular endothelial progenitors and differentiated vascular endothelial cells during early stages of vascular development. However, the *TgBAC(etv2:GFP)* line shows non-specific expression in the neural tube while the *Tg(−2.3 etv2:GFP)* line shows non-specific expression in epithelial and neuronal cells (Proulx et al., 2010; Davis et al., 2018). Furthermore, not all distal regulatory elements involved in the dynamic regulation of *etv2* expression may be present in these reporters.

CRISPR/Cas9-mediated knock-in approaches allow inserting a construct of interest into the endogenous gene locus, thus preserving regulatory elements that would be excluded by other methods of transgenesis. Knock-in strategies that utilize homologous recombination and homology-independent DNA repair have been previously reported in zebrafish embryos (Auer et al., 2014; Hoshijima et al., 2016). Here we performed CRISPR/Cas9-mediated knock-in of a targeting vector containing Gal4 transcriptional activator into the endogenous *etv2* locus. Using this approach, we generated the $etv2^{Gt(2A\text{-}Gal4)ci32}$ line (further referred to as $etv2^{ci32Gt}$), which, when crossed with the *Tg(UAS:EGFP)* line, shows highly specific GFP expression in vascular endothelial and hematopoietic cells. Due to an interruption of the *etv2* coding sequence, homozygous $etv2^{ci32Gt}$ embryos show strong defects in vascular development, allowing to visualize vascular progenitors in the *etv2* loss-of-function background. We further used these lines to analyze global transcriptional changes observed in $etv2^{ci32Gt}$ homozygous embryos, which resulted in identification of multiple novel candidate vascular endothelial and myeloid-specific genes. This reporter line will be a valuable tool for multiple researchers studying vascular and hematopoietic development.

RESULTS

Generation of *etv2*^{ci32Gt} zebrafish knock-in line.

To generate a reporter line, which would accurately label *etv2*-expressing cells in live zebrafish embryos, we employed a targeted knock-in approach. A highly efficient CRISPR / Cas9-mediated knock-in strategy has been previously reported, which utilizes homology-independent DNA repair (Auer et al., 2014). We designed and tested single-guide RNA (sgRNA) which targeted exon 5 of the *etv2* gene with nearly 100% efficiency (data not shown). Subsequently, we engineered a donor construct which contained *etv2* sgRNA bait sequence followed by the self-cleaving P2A peptide sequence fused to Gal4 transcriptional activator and polyadenylation sequence (Fig. 1). Integration of this construct in-frame with *etv2* coding sequence was expected to result in expression of the N-terminal fragment of Etv2 protein and a separate Gal4 protein. Although the N-terminal fragment of Etv2 was not expected to show any functional activity, heterozygous embryos were expected to be morphologically normal, while homozygous embryos should recapitulate the *etv2* loss-of-function phenotype due to the absence of full-length Etv2 protein.

A mixture containing *Cas9* mRNA, *etv2* sgRNA, and the *etv2* sgRNA-2A-Gal4 donor plasmid was injected into UAS:GFP transgenic embryos. A fraction of embryos showed mosaic GFP expression in vascular endothelial cells. Subsequently, the embryos were raised and fish progeny were screened for GFP expression. A founder was identified which produced embryos with specific GFP expression in the vasculature. The integration site was analyzed by PCR amplification and Sanger sequencing using genomic DNA isolated from GFP positive embryos. As expected, the P2A-Gal4 construct was specifically integrated in exon 5 of the *etv2* gene (Fig. 1). Unexpectedly, the predicted translation of the P2A-Gal4 was out of frame with the predicted translation of the *etv2* gene. It is possible that an alternative peptide can be produced from *etv2* mRNA in a different reading frame, which contains an upstream ATG codon. Alternatively, Gal4 translation may be initiated internally due to the presence of a strong Kozak sequence which was included in the construct design. To test for these possibilities, we designed *etv2–2A-GFP* reporter construct which contained 5'UTR of *etv2* gene, N-terminal portion of the Etv2 protein coding sequence and 2A-GFP sequence which was joined out-of-frame to the *etv2* coding sequence, precisely recapitulating the integration site present in *etv2*^{ci32Gt} embryos. Mutations in all four potentially-initiating ATG sites in the *etv2* coding sequence resulted in greatly increased GFP fluorescence compared to wt construct (Fig. 2). This suggests that there is a competing translation from both reading frames 1 and 2 present in embryos injected with the wild-type (wt) construct. Mutations that affect translation in frame 1 result in increased translation from frame 2. Mutation in the upstream ATG codon present in frame 2, as well as the ATG codon, which initiates GFP translation resulted in reduced fluorescence compared with the wt construct (Fig. 2). This suggests that translation from both ATG codons in frame 2 contributes to Gal4 expression in *etv2*^{ci32Gt} embryos.

In some cases CRISPR / Cas9 may cleave at off-target sites, which could result in the insertion of *2A-gal4* construct into additional sites within the zebrafish genome. We analyzed RNA-seq results obtained from *etv2*^{ci32Gt} heterozygous embryos at the 15-somite

stage (see Transcriptome analysis section below for additional details). All analyzed sequence reads that contained 2A-Gal4 sequence at the 5' end were fused to the same upstream *etv2* sequence. While this does not exclude the possibility of additional insertion sites, it shows that their contribution to GFP expression (if there was any) would be negligibly small.

etv2^{ci32Gt} knock-in line labels vascular endothelial and blood cells.

GFP expression was then analyzed in *etv2*^{ci32Gt} heterozygous embryos in *Tg(UAS:GFP)* background and compared with GFP expression in *Tg(−2.3 etv2:GFP)* and *TgBAC(etv2:GFP)* lines, as well as with the endogenous *etv2* expression pattern. Specific GFP expression in vascular endothelial progenitors in the cranial, trunk and tail regions was observed in both *etv2*^{ci32Gt}*; UAS:GFP* and *Tg(−2.3 etv2:GFP)* lines at the 14–21-somite stages, which was very similar to the endogenous *etv2* expression pattern analyzed by in situ hybridization (Fig. 3). *Tg(−2.3 etv2:GFP)* line also showed weak non-specific GFP expression in the epidermal cells which was not apparent in *etv2*^{ci32Gt}*; UAS:GFP* embryos. *etv2*^{ci32Gt}*; UAS:GFP* embryos were also much brighter compared to *Tg(−2.3 etv2:GFP)* embryos. *TgBAC (etv2:GFP)* line, as reported previously (Proulx et al., 2010), exhibited strong non-specific GFP expression in the neural tube which was absent in the other two lines (Fig. 3). At 24 hpf stage, GFP expression in the *etv2*^{ci32Gt}*; UAS:GFP* line was apparent in vascular endothelial cells of all blood vessels (Fig. 4). In addition, GFP expression was also present in red blood cells and macrophages, which did not show vascular endothelial mCherry expression when crossed to *kdrl:mCherry* line. The two other *etv2* reporter lines also exhibited similar expression patterns at this stage, except that *TgBAC(etv2:GFP)* line also exhibited non-specific neural tube expression (Fig. 4). Endogenous *etv2* expression was apparent in the vasculature but not red blood cells or macrophages (Fig. 4I). As we have suggested previously (Sumanas et al., 2008; Proulx et al., 2010), GFP fluorescence is observed in blood cells likely due to the perdurance of GFP protein; *etv2* is expressed in early hematopoietic progenitors but is downregulated as these cells differentiate.

Strong GFP expression in the entire vasculature continued throughout 2–7 dpf in *etv2*^{ci32Gt}*; UAS:GFP* and *TgBAC(etv2:GFP)* embryos (Fig. 5,6) and was also apparent in the tail fin vasculature of adult fish (data not shown). Both lines also showed GFP expression in the lymphatic vasculature (Fig. 6). We have previously reported similar although weaker *etv2* mRNA expression in the vasculature at 2–2.5 dpf (Davis et al., 2018). Although endogenous *etv2* expression in most blood vessels was largely not detectable at 3 dpf or later stages (data not shown), it is challenging to detect expression using whole-mount in situ hybridization in older embryos due to the limited probe penetration (see Discussion). In contrast, vascular endothelial specific expression in *Tg(−2.3 etv2:GFP)* line was downregulated between 48–72 hpf, while non-specific GFP expression in epithelial cells and a subset of neurons was apparent (Fig. 6). Endothelial expression was very weak or not apparent in this line at 5 dpf or later stages (data not shown). Overall, *etv2*^{ci32Gt}*; UAS:GFP* heterozygous embryos and adults were morphologically normal and did not have any apparent phenotypic defects.

etv2^{ci32Gt}*; UAS:GFP* homozygous embryos show vascular defects.

We then examined GFP expression in *etv2*^{ci32Gt}*; UAS:GFP* homozygous embryos which were expected to show the phenotype, associated with the loss of *etv2* function. As expected, *etv2* expression was nearly completely absent in *etv2*$^{ci32Gt-/-}$ embryos as analyzed by in situ hybridization at the 20-somite and 24 hpf stages (Fig. 7). Initiation of GFP expression in vascular and hematopoietic progenitors at or prior to the 10-somite stage did not appear to be affected in *etv2*^{ci32Gt}*; UAS:GFP* homozygous embryos (data not shown). However, GFP-positive putative vascular progenitors failed to migrate from the lateral plate mesoderm to the midline and did not coalesce into vascular cords at 14–22-somite stages (Fig. 8A,E, and data not shown). No intersegmental vessels (ISVs) were apparent at 24 hpf in *etv2*^{ci32Gt} homozygous embryos, although some ISV sprouts did emerge between 48–72 hpf (Fig. 8). These sprouts did not extend all the way and were misguided. Intriguingly, vascular defects in *etv2*^{ci32Gt} homozygous embryos between 48–72 hpf appeared more severe compared to the previously described *etv2*^{y11} allele and the *etv2* MO knockdown phenotype (Sumanas and Lin, 2006; Pham et al., 2007). Aside from these vascular defects, both *etv2*$^{ci32Gt+/-}$ and *etv2*$^{ci32Gt-/-}$ embryos appeared morphologically normal when analyzed using brightfield microscopy (Fig. 9).

In addition to GFP expression in vascular progenitors, GFP expression in multiple skeletal muscle cells was observed in *etv2*^{ci32Gt} homozygous embryos at the 20-somite and later stages (Fig. 8F,G, and data not shown). A few cells positive for muscle-specific GFP expression were also observed in *etv2*^{ci32Gt} heterozygous embryos. This expression may be caused by the transdifferentiation of multipotent vascular progenitors into skeletal muscle in the absence of *etv2* function, and will be explored in detail in a separate study (Chestnut et al, in review).

Transcriptome analysis in *etv2*^{ci32Gt} embryos.

To characterize changes in RNA transcriptome observed in *etv2*^{ci32Gt} homozygous embryos, we performed bulk RNA-seq analysis of *etv2*^{ci32Gt} heterozygous and homozygous embryos at the 15-somite and 24 hpf stages. Differential expression analysis detected 489 genes downregulated greater than two-fold in *etv2*^{ci32Gt} homozygous embryos at the 15-somite stage, and 170 genes downregulated greater than two-fold at 24 hpf (Table 1,2). This included many known vascular endothelial specific genes such as *gpr182, mrc1a, atgr2, aqp8a.1, lyve1b, stab2* and others, which have been previously shown to be regulated by *etv2* expression (Gomez et al., 2009; Wong et al., 2009). In addition, multiple myeloid specific markers including *ncf1, mmp13a, sla1a, srgn, mpx* and *mfap4* were greatly downregulated in *etv2*^{ci32Gt} homozygous embryos (Table 1,2). Downregulated vascular endothelial and myeloid markers were identified at both 15-somite and 24 hpf stages, and there was a significant overlap between affected genes at both stages. Overall, vascular endothelial genes showed greater downregulation at the 15-somite change, compared to 24 hpf. For example, *cdh5* expression in *etv2*^{ci32Gt} embryos was downregulated 27.1-fold at the 15-somite stage, and 2.4-fold at 24 hpf, while *kdr* was down 7.2 and 4.4-fold, and *fli1a* was down 2.1 and 1.3-fold, respectively. Downregulation of vascular endothelial and myeloid markers is consistent with the previously established *etv2* roles in vasculogenesis and myelopoiesis (Sumanas and Lin, 2006; Sumanas et al., 2008). *etv2* mutants undergo partial

recovery of vascular development at 24 hpf and later stages (Craig et al., 2015), therefore changes in gene expression are less pronounced at 24 hpf compared to the 15-somite stage. In addition to these established markers, multiple previously uncharacterized genes were downregulated in *etv2*^{ci32Gt} heterozygous embryos, suggesting that they may also exhibit vascular endothelial or myeloid expression. A complete list of downregulated and upregulated genes is provided in Suppl. Tables S1 and S2. Further experiments will be required to analyze their expression patterns and functional roles.

We then performed gene enrichment ontology (GO) analysis on downregulated and upregulated genes in *etv2*$^{ci32Gt-/-}$ embryos. Significantly changed GO terms of downregulated genes at both 15-somite stages and 24 hpf included ‘blood vessel development’, ‘blood vessel morphogenesis’ and ‘vasculature development’ (Tables 3 and 4). Several additional GO terms associated with hematopoietic and vascular development, such as ‘angiogenesis’, ‘hemangioblast cell differentiation’, ‘wound healing’ and ‘vasculogenesis’ were enriched in the dataset from the 15-somite stage embryos. In addition, GO terms commonly associated with the functions of vascular endothelial cells, including ‘blood coagulation’, ‘hemostasis’, ‘platelet activation’ were apparent from GO analysis at the 15-somite stage. Additional terms associated with vascular endothelial signaling or immunity including ‘angiotensin type II receptor pathway, ‘G-protein coupled peptide receptor pathway’, ‘leukocyte migration’ were associated with the genes downregulated at 24 hpf. In contrast, no GO terms were significantly enriched in upregulated genes at either 15-somite or 24 hpf stages in *etv2*^{ci32Gt} embryos. In addition, there was little overlap between upregulated genes at both stages (Suppl. Table S1 and S2), therefore the significance of upregulated genes is currently unclear.

DISCUSSION

In this study, we have established a novel *etv2*^{ci32Gt} knock-in reporter line which recapitulates well the endogenous *etv2* expression in vascular and hematopoietic progenitor cells. In addition, it enables visualization and study of *etv2*-deficient cells that would ordinarily express *etv2*. We demonstrate the utility of this line by performing differential transcriptomic analysis in *etv2*^{ci32Gt} heterozygous and homozygous embryos, which resulted in identification of multiple novel candidate genes that may function downstream of *etv2* during vasculogenesis and myelopoiesis.

Similar to the previously established *TgBAC(etv2:GFP)* and *Tg (−2.3 etv2:GFP)* lines (Proulx et al., 2010; Veldman and Lin, 2012), *etv2*^{ci32Gt}*; UAS:GFP line* shows GFP expression in vascular endothelial and hematopoietic progenitors. However, it does not show the neural tube expression which was observed in the *TgBAC(etv2:GFP)* line or the epithelial and neuronal expression observed in *Tg(−2.3etv2:GFP)* lines suggesting that these expression patterns were caused by either the absence, interruption or gain of certain regulatory enhancer elements in the previous lines. *UAS:GFP* expression was also significantly brighter compared to the GFP fluorescence in the *Tg(−2.3 etv2:GFP)* line which was generated by Tol2-mediated transgenesis, suggesting that GFP expression was amplified by the potent transcriptional activator Gal4 binding to multiple UAS sites. While *etv2* transcript is known to be downregulated in the vasculature by 24 hpf (Moore et al.,

2013; Craig et al., 2015), *etv2*^{ci32Gt}*; UAS:GFP* expression was bright and apparent throughout adulthood. Continued GFP fluorescence at 1–2 dpf could be explained by the perdurance of GFP, but this would not explain its persistence at later stages. We have previously reported that continued vascular endothelial *etv2* expression at lower levels is still apparent between 1.5–2.5 dpf (Davis et al., 2018). Whole mount in situ hybridization at later stages is typically challenging in zebrafish embryos due to poor probe penetration, therefore it is possible that *etv2* continues to be expressed at low levels in the vasculature throughout adulthood, and this low level expression is amplified in *etv2*^{ci32Gt}*; UAS:GFP* line. Alternatively, it is possible that the knock-in of this Gal4 construct has interrupted a regulatory element responsible for the downregulation of *etv2* at later stages.

Intriguingly, *etv2*^{ci32Gt} homozygous embryos show more severe vascular defects compared to the previously reported *etv2*^{y11} mutants and *etv2* MO embryos (Sumanas and Lin, 2006; Pham et al., 2007). Both *etv2*^{y11} and MO knockdown embryos show partial recovery of vascular defects between 1–3 dpf stages, due to the functional redundancy with *fli1b* gene, positioned adjacent to *etv2* on the same chromosome (Craig et al., 2015). This recovery is greatly compromised in *etv2*^{ci32Gt} homozygous embryos, resulting in a more severe phenotype. *etv2*^{y11} mutants are predicted to be null, which is supported by the loss of *etv2* mRNA expression due to nonsense-mediated RNA decay (NMRD) (Pham et al., 2007). NMRD is likely to trigger a compensatory response (El-Brolosy et al., 2019) in *etv2* mutants, which may not be observed in *etv2*^{ci32Gt} homozygous embryos, thus explaining the difference between these phenotypes. However, *etv2* MO embryos recapitulate *etv2*^{y11} phenotype very closely, and also show a similar recovery (Craig et al., 2015). An alternative possibility is that Gal4 insertion into the *etv2* locus has interrupted expression of a related *fli1b* gene which is positioned next to *etv2* on the same chromosome. Due to the vicinity of *etv2* and *fli1b* in the genome, the two genes are likely to share some regulatory elements. Indeed, *fli1b* expression is greatly downregulated in *etv2*$^{ci32Gt-/-}$ embryos based on our RNA-seq analysis (Suppl. Table S1, S2).

RNA-seq analysis confirmed the previously established role of *etv2* in vasculogenesis and myelopoiesis. In addition, it identified other novel genes, some of which may function as novel regulators of vascular development or myelopoiesis. Etv2 function is known to be evolutionarily conserved, and mouse *Etv2* mutants show loss of endothelial and hematopoietic differentiation (Lee et al., 2008; Ferdous et al., 2009). Whole transcriptome analysis using microarrays has been previously performed in murine *Flk1*+ cells sorted from *Etv2*-deficient embryoid bodies (Liu et al., 2012). Most vascular endothelial-specific genes identified in this study, including *Cdh5, Esam, Flt1, Tie1, Fli1, Erg, Lmo2* and others were also downregulated in zebrafish mutant embryos. In addition to endothelial defects, mouse *Etv2* mutants show loss red blood cell (RBC) differentiation (Lee et al., 2008), and loss of erythroid-specific gene expression was observed in *Etv2*-deficient embryoid bodies (Liu et al., 2012). In contrast, RBCs are still present in zebrafish *etv2*-deficient embryos (Sumanas and Lin, 2006), and there was no reduction observed in RBC gene expression based on our RNA-seq analysis. This could reflect differences in the regulation of erythropoiesis between zebrafish and murine embryos, or there may be additional redundancy between different Ets factors during zebrafish erythropoiesis. Upregulation of myocardial genes has been previously observed in *etv2*-deficient mouse embryoid bodies (Rasmussen et al., 2011; Liu

et al., 2012). Although we have previously shown that *etv2*-deficient cells can differentiate into cardiomyocytes in zebrafish embryos (Palencia-Desai et al., 2011), we did not see significant upregulation of myocardial genes in bulk RNA-seq analysis. It is possible that changes in myocardial expression are relatively small and difficult to detect using bulk RNA-seq analysis.

In summary, the *etv2*^{ci32Gt} line recapitulates the endogenous *etv2* expression during embryogenesis more accurately than previously generated reporter lines and will be a useful tool to study the mechanisms of vasculogenesis. Furthermore, transcriptomic analysis of *etv2*^{ci32Gt} embryos resulted in a comprehensive list of genes, expressed in vascular endothelial and myeloid cells, a function of which can be further interrogated in the future studies.

EXPERIMENTAL PROCEDURES

Zebrafish lines.

The following zebrafish lines were used in the study: *Tg(5xUAS:EGFP)* (Asakawa et al., 2008), *Tg(−2.3 etv2:GFP)*^{zf372} (Veldman and Lin, 2012), *TgBAC(etv2:GFP)*^{ci1} (Proulx et al., 2010), *Tg(kdrl:mCherry)*^{ci5} (Proulx et al., 2010). To generate *etv2*$^{Gt(2A\text{-}Gal4)ci32}$ knock-in line, a targeting construct was made by subcloning the *etv2* gRNA-P2A fragment (sequence: gggaaaggcccaagtcacagaggGGAAGCGGAGCTACTAACTTCAGCCTGCTGAAGCAGGCTGGAGACGTGGAGGAGAACCCTGGACCTgtcgacacc, *etv2* gRNA sequence is underlined, P2A sequence is in the upper case) into SalI-HindIII sites of the *flk1:Gal4VP16–2A-mCherry-pA-Tol2* construct (kindly donated by Drs. Naoki Mochizuki and Chunyue Yin; SalI-HindIII digest excised *flk1* promoter which was then replaced by the *etv2–2A* sequence). DNA fragment corresponding to *etv2* sgRNA was subcloned into the T7gRNA expression vector (Jao et al., 2013), which was linearized with BamHI and transcribed with T7 RNA polymerase (Promega). *Cas9* mRNA was synthesized from pT3TS-nCas9n vector (Jao et al., 2013) using T3 mMessage mMachine kit (ThermoFisher). A mixture of *Cas9* mRNA, *etv2* sgRNA and the *etv2-Gal4* targeting plasmid was injected into the *Tg(5xUAS:GFP)* zebrafish embryos at the 1-cell stage. Embryos showing any specific GFP expression were raised through adulthood. Approximately 50–100 adult fish were screened to identify a founder which produced progeny with a specific expression.

Throughout the study, embryos were typically incubated at 28.5 °C, except for the embryonic stages prior to 24 hpf, where embryos were incubated for part of the time at 23.5–24 °C to slow down their development. Embryos were staged using previously established criteria (Kimmel et al., 1995).

Genotyping primers.

Etv2-Gal4 insertion site was confirmed by PCR amplification and Sanger sequencing with the following primers: Etsrp-20-F: CCCCCTTAAGTTCCAGAAGG and

Gal4–1R: TCTTCAGACACTTGGCGCAC (see Fig. 1).

In situ hybridization.

In situ hybridization expression was performed as previously described (Jowett, 1999). Full-length *etv2* antisense probe was synthesized as previously described (Sumanas et al., 2005). To synthesize *etv2* probe which corresponds to the 3' portion of *etv2* gene (downstream of the Gal4 integration site), a construct containing full-length *etv2* cDNA in pSPORT1 was linearized with EciI. Antisense RNA was synthesized using SP6 RNA polymerase (Promega) and digoxygenin (DIG) labeling mix (Roche).

Reporter constructs and GFP fluorescence analysis.

Wild-type *etv2–2A-eGFP-pA* reporter construct was designed by fusing N-terminal portion of *etv2* and *2A-eGFP-pA* sequence to recapitulate the insertion site of *2A-Gal4*. The sequence was synthesized by Genscript (Piscataway, NJ, USA) and subcloned into the NotI site of pDB739 vector (Balciunas et al., 2006). Mutant variants of this sequence were produced by site-directed mutagenesis performed by Genscript. Wild-type and mutant variant constructs in pDB739 vector were linearized with XbaI, and mRNA was synthesized using SP6 mMessage mMachine Kit (ThermoFisher). 100 pg mRNA was injected at 1-cell stage, and embryos were kept at 23.5 °C overnight. Individual embryos were imaged in GFP channel at the 20-somite stage using AxioCam MRm grayscale camera (Zeiss), 10x objective (NA=0.3) and Axioimager compound fluorescent microscope (Zeiss). All embryos were imaged under the same exposure settings. Fluorescence intensity analysis was performed using Fiji / ImageJ software by choosing three different areas in each embryo along the trunk/tail outside of the yolk region and calculating integrated density. Background fluorescence was subtracted from each measurement. Average fluorescence values for each embryo were then calculated.

Confocal microscopy and image processing.

Embryos were mounted in 0.6% low melting point agarose and imaged using a Nikon A1 confocal microscope at the CCHMC Confocal Imaging Core. Images of embryos older than 1 dpf were obtained by imaging 2–3 embryonic regions separately and stitching individual images with Nikon Elements software. Image levels were adjusted using Adobe Photoshop CS6 to increase the contrast. Acquisition gain and laser intensity settings were adjusted based on the fluorescence intensity of individual embryos, therefore embryos from different reporter lines were not imaged under the same settings.

RNA-seq analysis.

etv2^{ci32Gt} heterozygous and homozygous embryos were obtained from the incross of *etv2*$^{ci32Gt+/-}$*; UAS:GFP* carriers and sorted based on GFP expression pattern. Criteria for selecting *etv2*$^{ci32Gt-/-}$ embryos included disorganized GFP expression in the trunk region and ectopically located GFP-positive cells positioned within the somites at the 15-somite stage, and the absence of intersegmental vessels at 24 hpf. Genotype of sorted embryos was confirmed by either in situ hybridization analysis for *etv2* expression in selected embryos (Fig. 7) or subsequent analysis of RNA-seq results, which showed absence of C-terminal *etv2* sequence reads in *etv2*$^{ci32Gt-/-}$ embryos (data not shown). 3 batches of 15–20 heterozygous and homozygous embryos were frozen at the 15-somite and 24 hpf stages.

Bulk RNA was purified using RNA-quous 4-PCR kit (ThermoFisher). Library synthesis and next generation RNA sequencing (20M PE-150 reads) was performed by Novogene, Inc; each stage contained triplicate samples. Sequences were aligned to the Zv9 zebrafish genome, and RNA-seq analysis was performed using Strand 3.0 software package. Gene list was filtered to retain genes which have >10 total reads in all samples in any of the genotypes (heterozygous or homozygous). Additional filtering for $p<0.05$ was performed for the gene list shown in Tables 1 and 2. GO term analysis was performed using Strand 3.0 with the significance cut off p (adjusted)<0.05.

To analyze Gal4 insertion sites, Next Gen sequence files were opened with Mac TextEdit software, and 2A-Gal4 sequences were identified using the search function. Adjacent upstream sequence was then manually inspected. In all 50 cases analyzed, it perfectly matched the same upstream sequence within the *etv2* gene.

RNA-seq files have been uploaded to the NCBI Gene Expression Omnibus (GEO) database and can be located under the accession number GSE139108.

Supplementary Material

Refer to Web version on PubMed Central for supplementary material.

Acknowledgements.

This research was supported by the NIH R21 AI128445 and RIP award from Cincinnati Children's Research Foundation to S.S. We thank Tiffany Duong who was involved in making Etv2-Gal4 targeting construct and Matt Kofron for help with imaging at the CCHMC Confocal Microscopy Core.

REFERENCES

Asakawa K, Suster ML, Mizusawa K, Nagayoshi S, Kotani T, Urasaki A, Kishimoto Y, Hibi M, Kawakami K. 2008 Genetic dissection of neural circuits by Tol2 transposon-mediated Gal4 gene and enhancer trapping in zebrafish. Proc Natl Acad Sci U S A 105:1255–1260. [PubMed: 18202183]

Auer TO, Duroure K, De Cian A, Concordet JP, Del Bene F. 2014 Highly efficient CRISPR/Cas9-mediated knock-in in zebrafish by homology-independent DNA repair. Genome Res 24:142–153. [PubMed: 24179142]

Balciunas D, Wangensteen KJ, Wilber A, Bell J, Geurts A, Sivasubbu S, Wang X, Hackett PB, Largaespada DA, McIvor RS, Ekker SC. 2006 Harnessing a high cargo-capacity transposon for genetic applications in vertebrates. PLoS Genet 2:e169. [PubMed: 17096595]

Craig MP, Grajevskaja V, Liao HK, Balciuniene J, Ekker SC, Park JS, Essner JJ, Balciunas D, Sumanas S. 2015 Etv2 and fli1b function together as key regulators of vasculogenesis and angiogenesis. Arterioscler Thromb Vasc Biol 35:865–876. [PubMed: 25722433]

Davis JA, Koenig AL, Lubert A, Chestnut B, Liu F, Palencia Desai S, Winkler T, Pociute K, Choi K, Sumanas S. 2018 ETS transcription factor Etsrp / Etv2 is required for lymphangiogenesis and directly regulates vegfr3 / flt4 expression. Dev Biol 440:40–52. [PubMed: 29753018]

El-Brolosy MA, Kontarakis Z, Rossi A, Kuenne C, Gunther S, Fukuda N, Kikhi K, Boezio GLM, Takacs CM, Lai SL, Fukuda R, Gerri C, Giraldez AJ, Stainier DYR. 2019 Genetic compensation triggered by mutant mRNA degradation. Nature 568:193–197. [PubMed: 30944477]

Ferdous A, Caprioli A, Iacovino M, Martin CM, Morris J, Richardson JA, Latif S, Hammer RE, Harvey RP, Olson EN, Kyba M, Garry DJ. 2009 Nkx2–5 transactivates the Ets-related protein 71 gene and specifies an endothelial/endocardial fate in the developing embryo. Proc Natl Acad Sci U S A 106:814–819. [PubMed: 19129488]

Gomez GA, Veldman MB, Zhao Y, Burgess S, Lin S. 2009 Discovery and characterization of novel vascular and hematopoietic genes downstream of etsrp in zebrafish. PLoS One 4:e4994. [PubMed: 19308258]

Hoshijima K, Jurynec MJ, Grunwald DJ. 2016 Precise Editing of the Zebrafish Genome Made Simple and Efficient. Dev Cell 36:654–667. [PubMed: 27003937]

Jao LE, Wente SR, Chen W. 2013 Efficient multiplex biallelic zebrafish genome editing using a CRISPR nuclease system. Proc Natl Acad Sci U S A 110:13904–13909. [PubMed: 23918387]

Jowett T. 1999 Analysis of protein and gene expression. Methods Cell Biol 59:63–85. [PubMed: 9891356]

Kimmel CB, Ballard WW, Kimmel SR, Ullmann B, Schilling TF. 1995 Stages of embryonic development of the zebrafish. Dev Dyn 203:253–310. [PubMed: 8589427]

Lee D, Park C, Lee H, Lugus JJ, Kim SH, Arentson E, Chung YS, Gomez G, Kyba M, Lin S, Janknecht R, Lim DS, Choi K. 2008 ER71 acts downstream of BMP, Notch, and Wnt signaling in blood and vessel progenitor specification. Cell Stem Cell 2:497–507. [PubMed: 18462699]

Liu F, Kang I, Park C, Chang LW, Wang W, Lee D, Lim DS, Vittet D, Nerbonne JM, Choi K. 2012 ER71 specifies Flk-1+ hemangiogenic mesoderm by inhibiting cardiac mesoderm and Wnt signaling. Blood 119:3295–3305. [PubMed: 22343916]

Moore JC, Sheppard-Tindell S, Shestopalov IA, Yamazoe S, Chen JK, Lawson ND. 2013 Post-transcriptional mechanisms contribute to Etv2 repression during vascular development. Dev Biol 384:128–140. [PubMed: 24036310]

Palencia-Desai S, Kohli V, Kang J, Chi NC, Black BL, Sumanas S. 2011 Vascular endothelial and endocardial progenitors differentiate as cardiomyocytes in the absence of Etsrp/Etv2 function. Development 138:4721–4732. [PubMed: 21989916]

Pham VN, Lawson ND, Mugford JW, Dye L, Castranova D, Lo B, Weinstein BM. 2007 Combinatorial function of ETS transcription factors in the developing vasculature. Dev Biol 303:772–783. [PubMed: 17125762]

Proulx K, Lu A, Sumanas S. 2010 Cranial vasculature in zebrafish forms by angioblast cluster-derived angiogenesis. Dev Biol.

Rasmussen TL, Kweon J, Diekmann MA, Belema-Bedada F, Song Q, Bowlin K, Shi X, Ferdous A, Li T, Kyba M, Metzger JM, Koyano-Nakagawa N, Garry DJ. 2011 ER71 directs mesodermal fate decisions during embryogenesis. Development 138:4801–4812. [PubMed: 21989919]

Sumanas S, Gomez G, Zhao Y, Park C, Choi K, Lin S. 2008 Interplay among Etsrp/ER71, Scl, and Alk8 signaling controls endothelial and myeloid cell formation. Blood 111:4500–4510. [PubMed: 18270322]

Sumanas S, Jorniak T, Lin S. 2005 Identification of novel vascular endothelial-specific genes by the microarray analysis of the zebrafish cloche mutants. Blood 106:534–541. [PubMed: 15802528]

Sumanas S, Lin S. 2006 Ets1-related protein is a key regulator of vasculogenesis in zebrafish. PLoS Biol 4:e10. [PubMed: 16336046]

Veldman MB, Lin S. 2012 Etsrp/Etv2 is directly regulated by Foxc1a/b in the zebrafish angioblast. Circ Res 110:220–229. [PubMed: 22135404]

Wong KS, Proulx K, Rost MS, Sumanas S. 2009 Identification of vasculature-specific genes by microarray analysis of Etsrp/Etv2 overexpressing zebrafish embryos. Dev Dyn 238:1836–1850. [PubMed: 19504456]

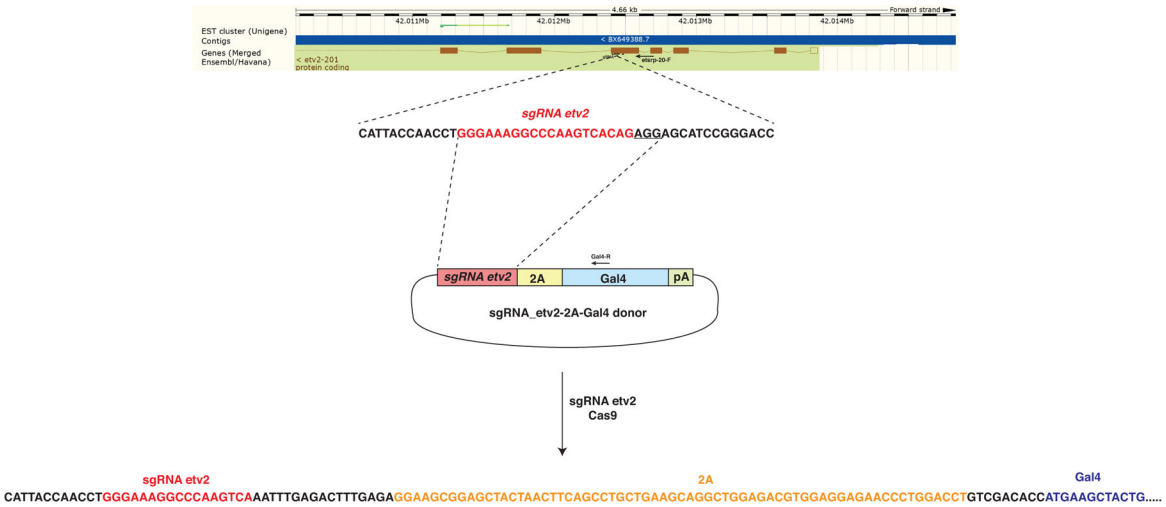

Figure 1.

A diagram of *sgRNA-2A-Gal4* construct and its insertion into the *etv2* genomic locus. The targeting construct contained *etv2* sgRNA site, followed by in-frame fusion to the viral peptide P2A, a transcriptional activator Gal4 and the SV40 polyA sequence. *etv2* sgRNA targets the fifth exon of *etv2* genomic sequence. The diagram shows approximate locations (not to scale) of the primers used for PCR amplification and sequencing.

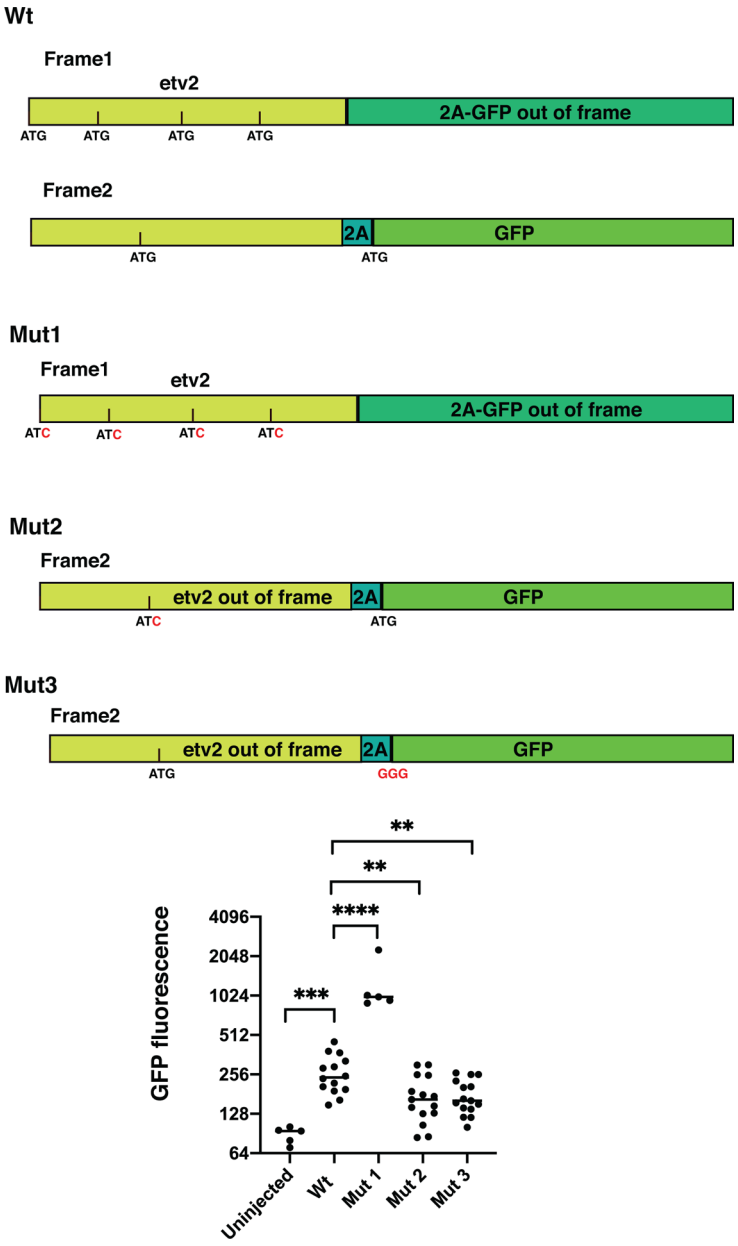

Figure 2.

Effect of different mutations on expression of the *etv2-2A-GFP* reporter. The reporter was designed to mimic the insertion of 2A-Gal4 into the genomic *etv2* locus. Wild-type (wt) construct contains 5'UTR and the N-terminal coding sequence of the *etv2* gene, and 2A-GFP sequence inserted out-of-frame. Four potential translation-initiating ATG sequences are shown in Frame 1. Frame 2 contains a single initiating ATG which is in-frame with 2A-GFP translation. Mutant 1 (Mut1) has mutations in all four ATG sites present in frame 1. Mutant 2 (Mut2) has mutation in the ATG site within the frame 2. Mutant 3 (Mut3) has a mutation within the ATG sequence that initiates GFP translation. The scatter plot shows relative GFP fluorescence intensity values (plotted in $\log_2$ scale) of embryos injected with different *etv2–2A-GFP* reporter constructs. Note increased GFP fluorescence in embryos injected with

Mut1 construct and reduced expression in Mut2 and Mut3-injected embryos compared to embryos injected with the wt construct. ** $p<0.01$, *** $p<0.001$, ****$p<0.0001$, t-Student's test (two-tailed).

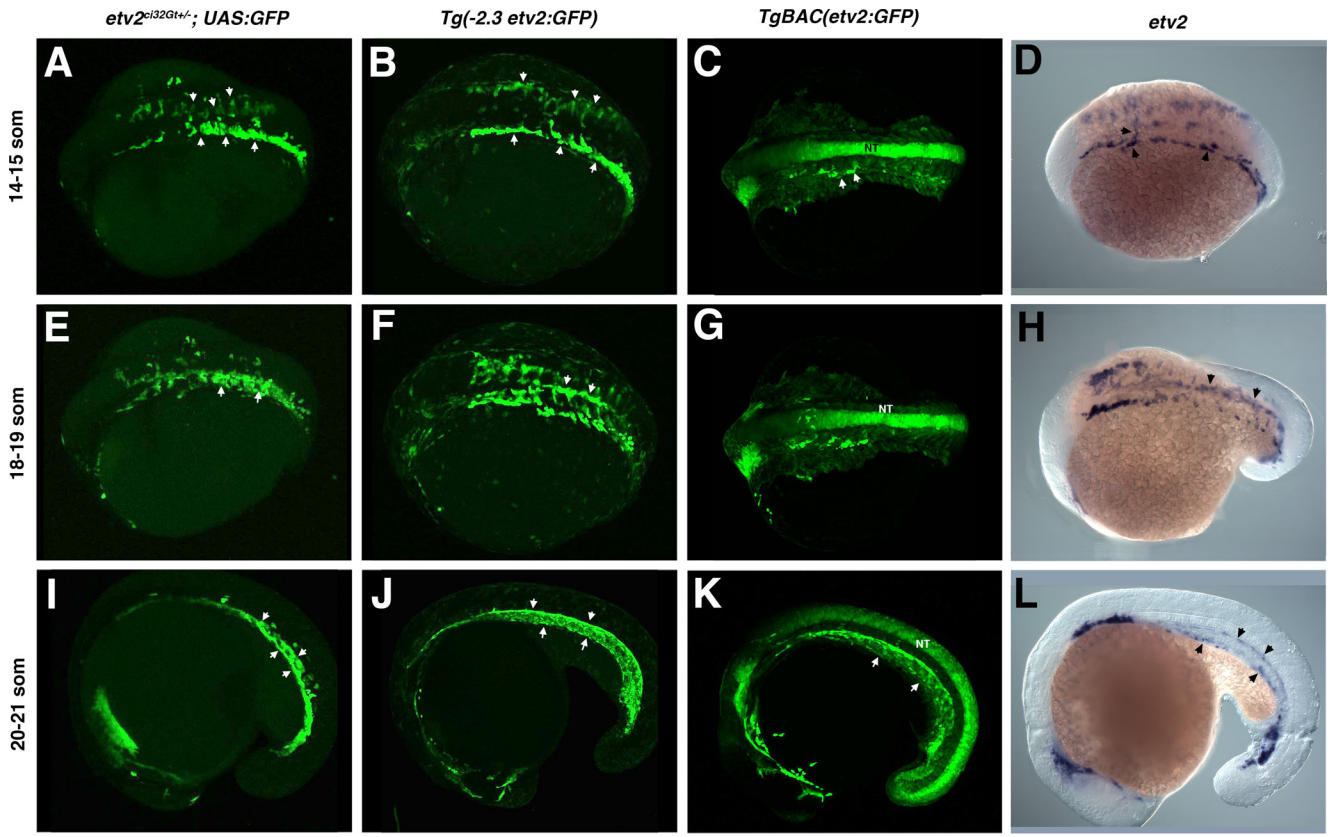

Figure 3.

A comparison of *etv2*$^{ci32Gt+/-}$*; UAS:GFP, Tg(−2.3etv2:GFP), TgBAC(etv2:GFP)* fluorescence pattern and *etv2* mRNA expression analyzed by in situ hybridization (ISH) at the 14–21 somite stages. (A-C) GFP fluorescence or (D) *etv2* mRNA expression is apparent in bilaterally located vascular endothelial progenitors which have started migrating towards the midline at the 14–15-somite stages (arrowheads). Strong non-specific GFP expression in the neural tube (NT) is apparent in *TgBAC(etv2:GFP)* embryos. (E-H) GFP-positive vascular endothelial progenitors at the 18–19-somite stages are coalescing at the midline into vascular cords (arrowheads, E,F). Similar *etv2* expression pattern is observed by ISH analysis (H). (I-L) GFP expression at the 20–21-somite stages is apparent in the forming axial vasculature (arrowheads), and non-specific expression is apparent in the neural tube (K). Similar *etv2* expression pattern is apparent from ISH analysis (L). A-H, dorsal or dorso-lateral view; I-L, lateral view, anterior is to the left.

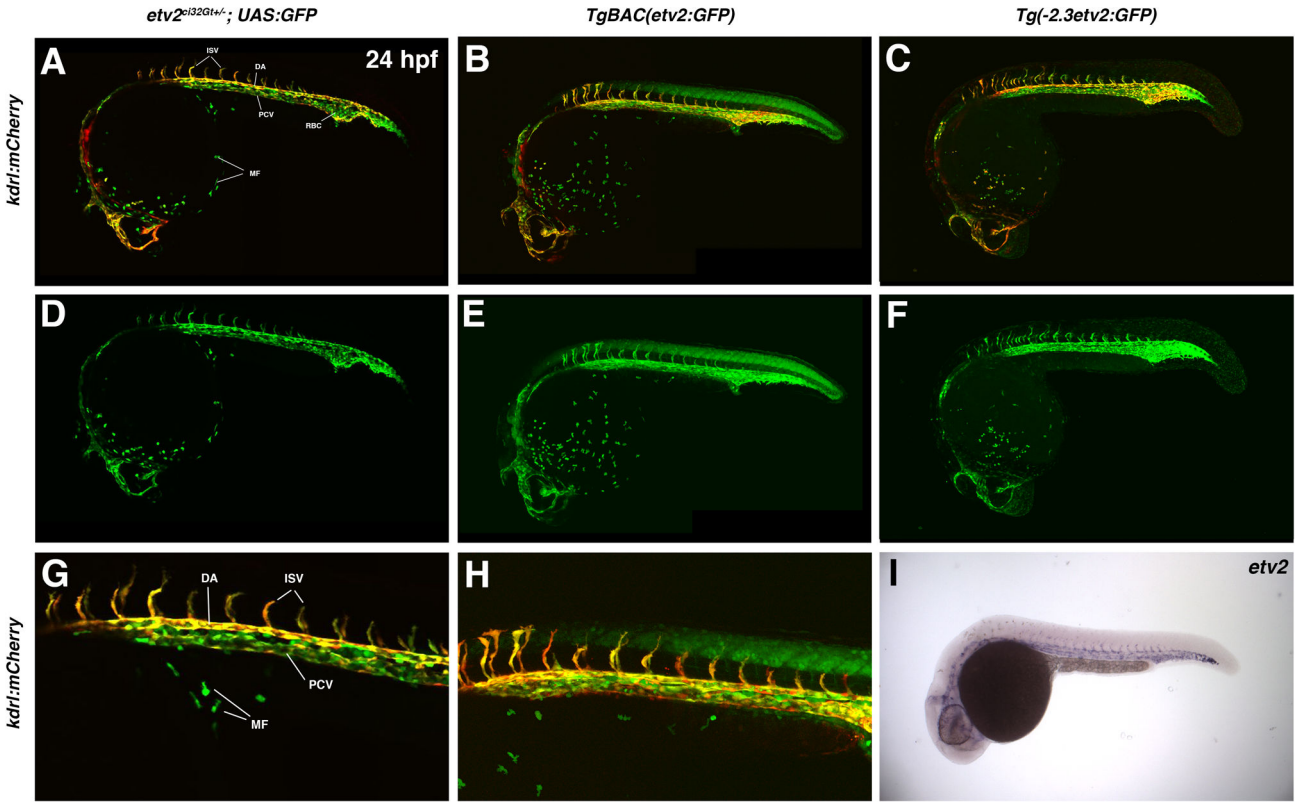

Figure 4.

A comparison of *etv2*$^{ci32Gt+/-}$*; UAS:GFP*, *TgBAC(etv2:GFP)*, *Tg(−2.3etv2:GFP)* fluorescence pattern (in *kdrl:mCherry* background, top row) and *etv2* mRNA expression analyzed by in situ hybridization (ISH) at 24 hpf. *etv2*$^{ci32Gt+/-}$*; UAS:GFP* expression is apparent throughout the entire vasculature, red blood cells (RBC) and macrophages (MF). *TgBAC(etv2:GFP)* shows similar expression pattern, and also shows non-specific expression in the neural tube. (A-C) Merged mCherry and GFP channels; (D-F) GFP channel; (G,H) magnified images of the trunk region in (A,B). (I) ISH analysis for *etv2* mRNA expression at 24 hpf. DA, dorsal aorta; PCV, posterior cardinal vein; ISV, intersegmental vessels.

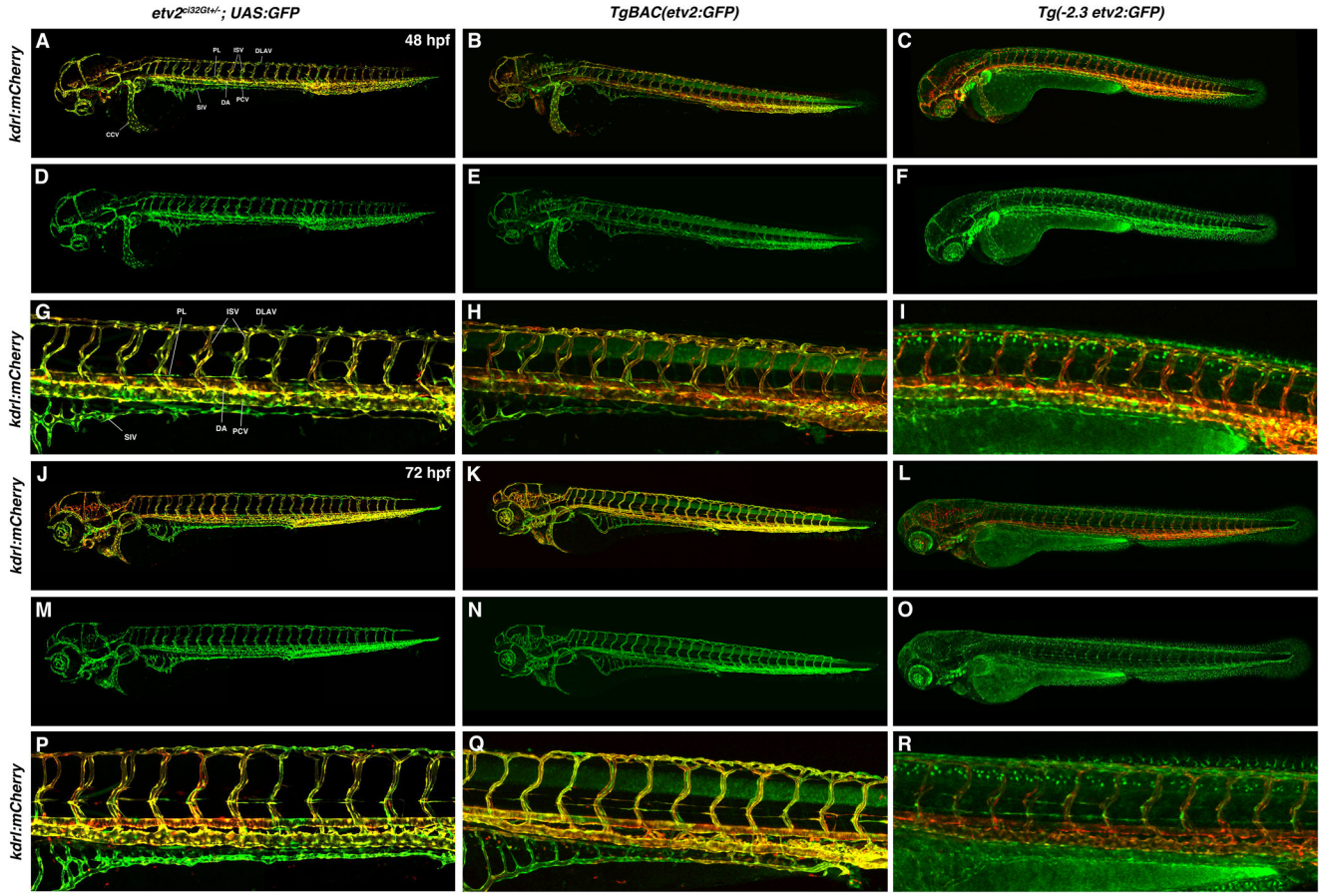

Figure 5.

A comparison of *etv2*$^{ci32Gt+/-}$*; UAS:GFP*, *TgBAC(etv2:GFP), Tg(−2.3etv2:GFP)* fluorescence pattern (in *kdrl:mCherry* background) at 48 hpf (A-I) and 72 hpf (J-R). *etv2*$^{ci32Gt+/-}$*; UAS:GFP* expression is apparent throughout the entire vasculature and in lymphatic progenitors (parachordal lymphangioblasts, PLs). *TgBAC(etv2:GFP)* shows similar expression pattern, and also shows non-specific expression in the neural tube. Vascular endothelial expression in *Tg(−2.3etv2:GFP)* line is downregulated after 48 hpf and is very weak at 72 hpf, while non-specific epithelial expression is apparent. (A-C, J-L) Merged mCherry and GFP channels; (D-F, M-O) GFP channel; (G-I, P-R) magnified images of the trunk region in (A-C, J-L). DA, dorsal aorta; PCV, posterior cardinal vein; ISV, intersegmental vessels, SIV, subintestinal vessel; DLAV, dorsal longitudinal anastomotic vessel; CCV, common cardinal vein.

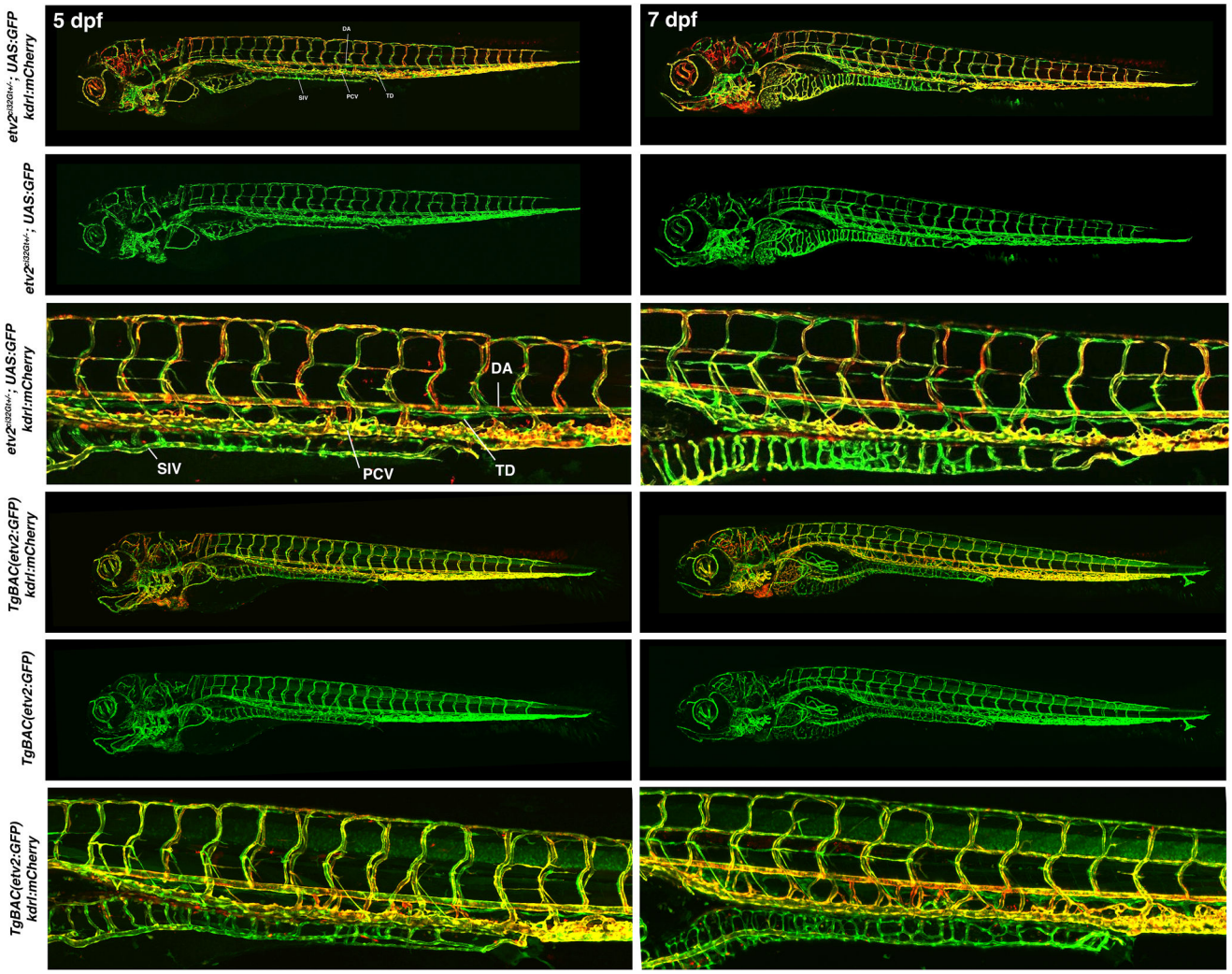

Figure 6.

A comparison of *etv2*$^{ci32Gt+/-}$*; UAS:GFP* and *TgBAC(etv2:GFP)* embryos in *kdrl:mCherry* background at 5 and 7 dpf. Both lines show GFP expression in the entire vasculature and lymphatics. DA, dorsal aorta; PCV, posterior cardinal vein; SIV, subintestinal vein (thoracic duct, TD). *Tg (−2.3etv2:GFP)* line did not show vascular endothelial expression at these stages.

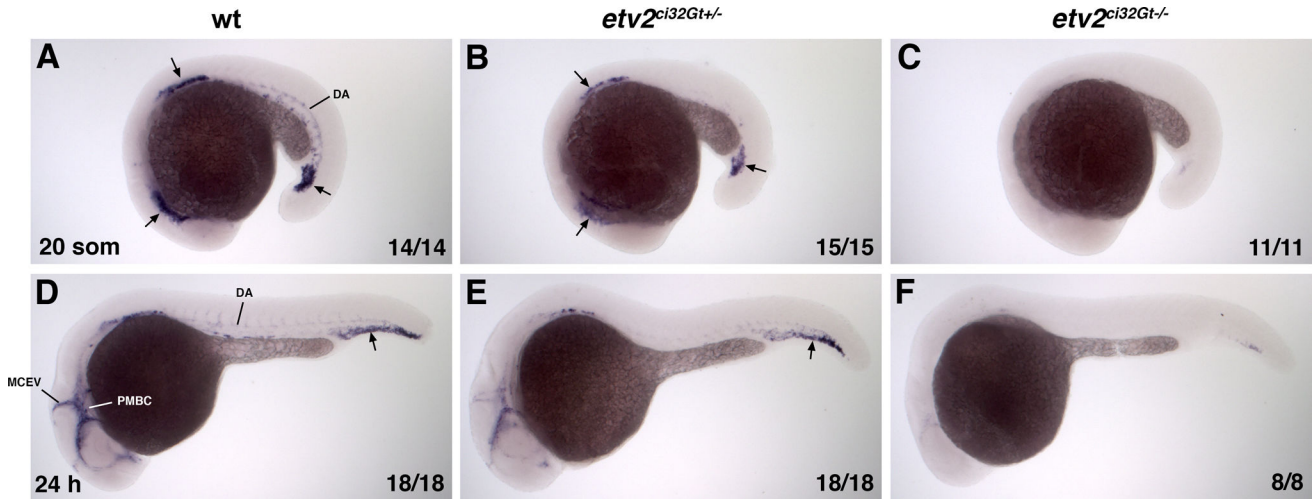

Figure 7.

etv2 expression analysis in wild-type, *etv2*$^{ci32G+-/-}$ and *etv2*$^{ci32Gt-/-}$ embryos at the 20-somite (A-C) and 24 hpf stages (D-F). Embryos were obtained from an incross of *etv2*$^{ci32Gt+/-}$*; UAS:GFP*$^{+/+}$ parents and sorted based on their GFP fluorescence pattern. Antisense *etv2* RNA probe which corresponds to the C-terminal portion of the *etv2* coding sequence and 3'UTR downstream of the Gal4 insertion side was used for in situ hybridization (see Experimental Procedures). (A-C) In non-fluorescent wild-type siblings (wt), strong *etv2* expression is apparent in vascular progenitors in the anterior lateral plate mesoderm, presumptive progenitors of the anterior and common cardinal veins, and in vascular progenitors next to the tailbud (arrows). Weaker expression in the dorsal aorta (DA) is also apparent. Note the reduced *etv2* expression in *etv2*$^{ci32Gt+/-}$ embryos and nearly absent expression in *etv2*$^{ci32Gt-/-}$ embryos. (D-F) In wild-type siblings, strong *etv2* expression is apparent in the cranial venous vasculature, including the primordial midbrain channel (PMBC) and the middle cerebral vein (MCEV), as well as the tail plexus region (arrow). Weaker expression in the DA is also apparent. Note the reduced *etv2* expression in *etv2*$^{ci32Gt+/-}$ embryos and nearly absent expression in *etv2*$^{ci32Gt-/-}$ embryos.

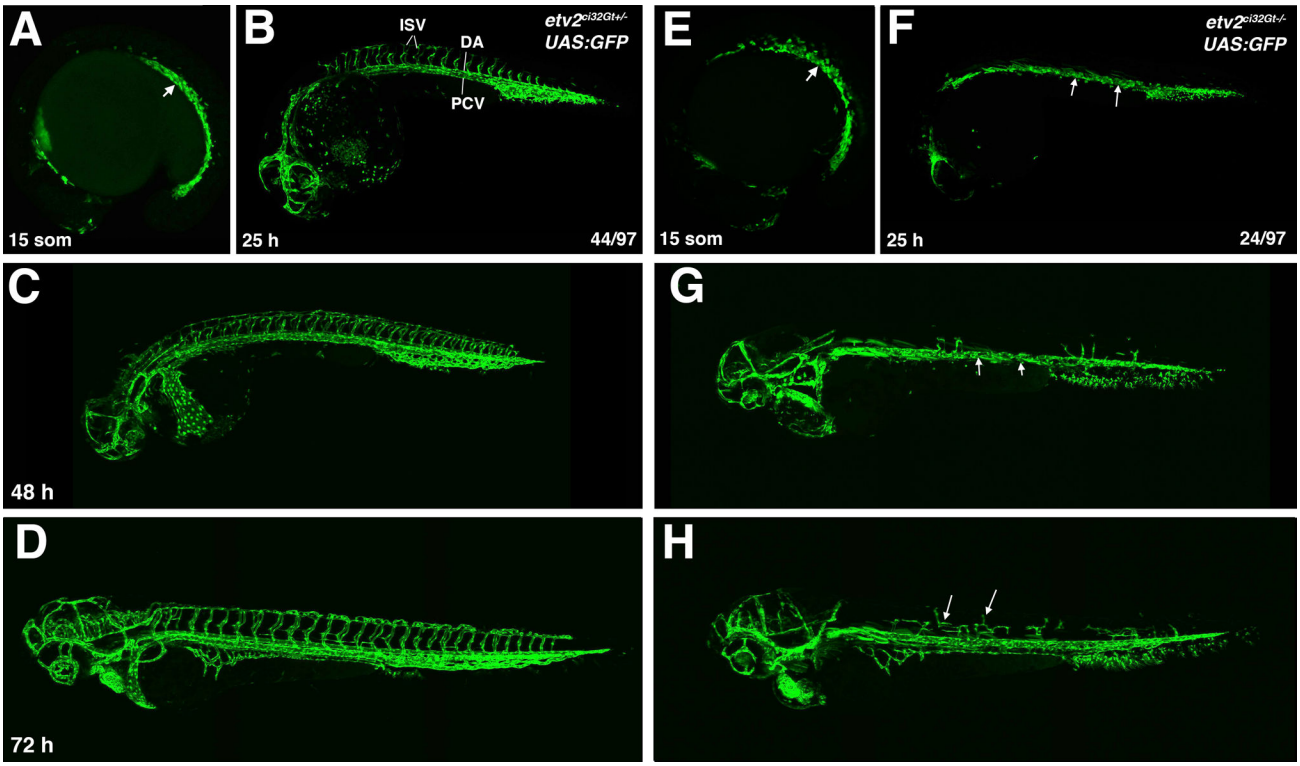

Figure 8.

A comparison of vascular development in heterozygous *etv2*$^{ci32Gt+/-}$*; UAS:GFP* and homozygous *etv2*$^{ci32Gt-/-}$*; UAS:GFP* embryos. GFP expression is apparent in vascular progenitors of the trunk axial vasculature (arrow, A) in *etv2*$^{ci32Gt+/-}$*; UAS:GFP* embryos. This domain is broader and disorganized in *etv2*$^{ci32Gt-/-}$*; UAS:GFP* embryos (E). Vascular progenitors fail to coalesce into vascular cords in *etv2*$^{ci32Gt-/-}$*; UAS:GFP* embryos at 25 hpf (arrows, F, compare with C). Intersegmental vessels (ISVs) are absent in *etv2*$^{ci32Gt-/-}$*; UAS:GFP* embryos between 25–48 hpf (F,G). Some ISV sprouts are apparent at 72 hpf but are shorter and mispatterned (H, arrows).

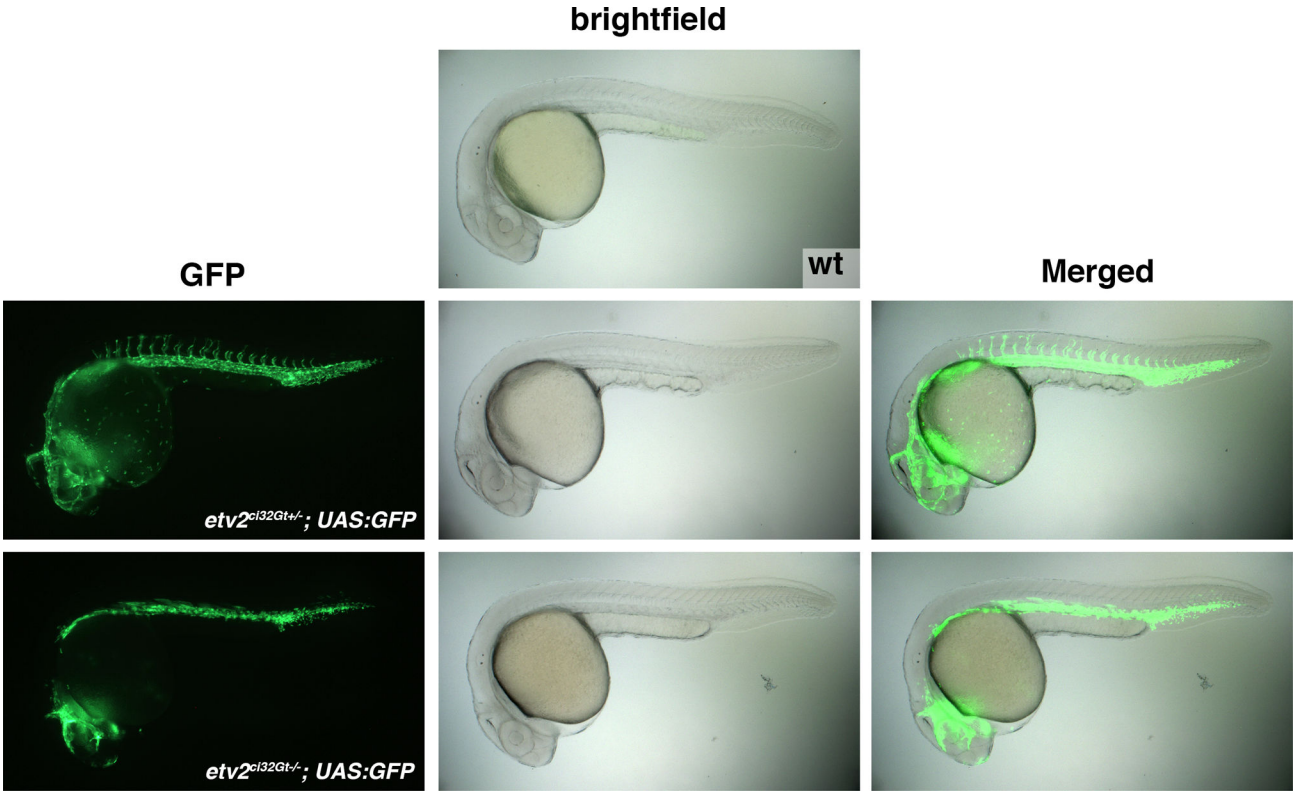

Figure 9.

Brightfield and fluorescent images of *etv2*$^{ci32Gt+/-}$ and *etv2*$^{ci32Gt-/-}$ embryos and their non-fluorescent wild-type siblings at 24 hpf. No morphological defects are apparent in the brightfield images of *etv2*$^{ci32Gt+/-}$ and *etv2*$^{ci32Gt-/-}$ embryos.

Table 1.

Top 50 downregulated genes in *etv2*^{ci32Gt} homozygous embryos compared to *etv2*^{ci32Gt} heterozygous embryos at the 15-somite stage and their reported expression patterns.

Gene Symbol	Fold change	p	Expression pattern
gpr182	−82.52	4.95E-04	endothelial
mrc1a	−62.69	1.36E-03	endothelial
agtr2	−62.49	2.23E-05	endothelial
ncf1	−47.43	5.26E-06	macrophage, neutrophil
mmp13a	−40.14	2.13E-04	macrophage
flt1	−37.79	2.36E-03	endothelial
zgc:66382	−34.46	4.76E-03	exocrine pancreas
CABZ01018247.1 (pecam1)	−27.82	2.65E-06	endothelial
cdh5	−27.12	2.20E-03	endothelial
clec14a	−26.57	1.87E-05	endothelial
scarf1	−21.96	1.49E-05	endothelial
tie1	−21.80	5.42E-05	endothelial
si:zfos-1697h8.1	−19.97	8.50E-05	unknown
RASIP1	−18.60	2.94E-05	endothelial
CD93	−17.85	2.91E-04	endothelial
sla1a	−14.36	1.12E-03	macrophage
myct1a	−13.88	1.33E-02	endothelial
shank3b	−13.41	1.67E-04	brain
cldn5b	−12.99	6.83E-04	endothelial
INPP5D	−11.35	9.24E-03	neutrophil
sox7	−9.97	2.45E-05	endothelial
erg	−9.92	1.13E-04	endothelial
zgc:171534	−9.82	1.39E-02	unknown
si:dkey-80c24.1	−9.63	1.87E-03	unknown
samsn1a	−9.48	7.95E-03	blood, macrophage
epdl2	−9.02	3.64E-02	unknown
dusp5	−8.63	4.65E-04	endothelial
tagap	−8.57	2.64E-02	endothelial
KLHL4	−8.49	1.28E-02	endothelial
pde6c	−8.47	1.96E-02	retina
PTPN6	−7.90	5.62E-03	macrophage
timd4	−7.54	1.01E-02	unknown
sod3a	−7.46	3.96E-03	ubiquitous
CABZ01086927.1	−7.36	5.41E-04	unknown
kdr	−7.18	1.56E-03	endothelial
etv2	−7.09	5.65E-06	endothelial

Gene Symbol	Fold change	p	Expression pattern
ARHGEF9 (1 of 3)	−7.09	2.15E-02	endothelial
comtd1	−6.85	1.08E-02	liver, oligodendrocyte
CABZ01007930.1 (cldn34a)	−6.85	4.85E-02	unknown
sele	−6.84	6.76E-04	endothelial
GOLT1A	−6.63	1.49E-02	unknown
si:ch73–248e21.5	−6.56	4.29E-02	unknown
arhgef9b	−6.16	2.25E-04	endothelial
plbd1	−6.15	2.37E-03	yolk syncytial layer
si:dkey-241l7.2 (REG4)	−5.99	4.01E-02	unknown
akr1a1a	−5.91	4.86E-03	ubiquitous
ITGB2	−5.79	8.11E-03	unknown
pcxb	−5.79	4.43E-03	ubiquitous
aqp8a.1	−5.66	1.00E-04	endothelial
cxcr3.2	−5.51	2.69E-03	macrophage

Table 2.

Top 50 downregulated genes in *etv2*^{ci32Gt} homozygous embryos compared to *etv2*^{ci32Gt} heterozygous embryos at 24 hpf stage and their reported expression patterns.

Gene Symbol	FC	p	Expression pattern
aqp8a.1	−83.83	2.39E-04	endothelial
mfap4	−31.63	1.78E-03	macrophage
samsn1a	−24.75	3.67E-04	blood / macrophage
lyve1b	−21.35	1.55E-02	endothelial
il13ra2	−20.19	1.20E-03	endothelial
srgn	−19.58	1.09E-03	neutrophil
MFAP4 (13 of 13)	−16.22	4.61E-03	macrophage
slc22a7b	−14.61	2.53E-03	unknown
MFAP4 (4 of 13)	−14.48	5.21E-03	macrophage
mpx	−12.55	2.01E-02	neutrophil
ITGAE	−11.78	4.21E-03	unknown
havcr1	−9.40	5.90E-03	macrophage
mrc1a	−9.28	2.14E-04	endothelial
grap2b	−9.22	2.47E-02	macrophage (likely)
spi1l	−9.11	3.91E-03	macrophage, neutrophil
etv2	−8.88	2.39E-04	endothelial
stab2	−8.63	1.97E-06	endothelial
notchl	−8.61	2.73E-02	unknown
si:dkey-207j16.5	−8.40	1.66E-02	unknown
ncf1	−8.35	1.06E-02	macrophage, neutrophil
gpr182	−8.08	7.88E-05	endothelial
ppp1r18	−7.91	2.15E-02	unknown
cxcr3.2	−7.80	9.22E-04	macrophage
vsg1	−7.63	4.94E-06	endothelial
tie1	−7.51	4.01E-04	endothelial
lyz	−7.48	1.26E-04	macrophage, neutrophil
CR384059.1	−7.28	9.30E-03	unknown
flt1	−6.94	2.75E-04	endothelial
fgd5b	−6.46	1.93E-02	unknown
cldn5b	−6.34	5.42E-05	endothelial
ANPEP (5 of 5)	−6.32	1.40E-02	unknown
csf1rb	−6.15	1.72E-02	microglial
CABZ01018247.1 (pecam1)	−5.99	1.38E-03	endothelial
dennd2db	−5.91	4.83E-02	ubiquitous
CD93	−5.79	1.19E-03	endothelial
erg	−5.61	3.07E-04	endothelial

Gene Symbol	FC	p	Expression pattern
si:ch211–145b13.6	−5.47	3.38E-02	unknown
si:ch211–13o20.1	−5.31	4.54E-03	unknown
irf8	−5.31	7.25E-03	macrophage
tie2	−5.14	1.13E-06	endothelial
vtg3	−4.97	1.62E-03	multiple tissues
CU463231.1	−4.77	2.87E-02	unknown
zgc:66382	−4.67	2.55E-02	exocrine pancreas
si:ch211–149k23.9	−4.51	1.74E-02	unknown
kdr	−4.45	2.23E-04	endothelial
si:ch211–278p9.4	−4.09	1.65E-02	unknown
zp2l1	−3.93	4.37E-02	unknown
CCM2L	−3.81	2.10E-02	endothelial
cybb	−3.77	2.29E-03	neutrophil
micall2a	−3.74	1.33E-03	endothelial

Table 3.

Gene ontology (GO) term enrichment analysis using downregulated genes in *etv2*$^{ci32Gt-/-}$ embryos at the 15-somite stage.

GO ACCESSION	GO Term	corrected p-value
GO:0008150|GO:0000004|GO:0007582	biological_process	8.26E-14
GO:0055114	oxidation-reduction process	2.20E-07
GO:0044699	single-organism process	1.12E-06
GO:0050817	**coagulation**	1.12E-06
GO:0070011	peptidase activity, acting on L-amino acid peptides	1.12E-06
GO:0007596	**blood coagulation**	1.12E-06
GO:0016491	oxidoreductase activity	1.12E-06
GO:0008233	peptidase activity	1.23E-06
GO:0007599	**hemostasis**	1.34E-06
GO:0003824	catalytic activity	2.50E-06
GO:0050878	regulation of body fluid levels	2.50E-06
GO:0008234|GO:0004220	cysteine-type peptidase activity	3.55E-06
GO:0005576	extracellular region	5.13E-06
GO:0006869	lipid transport	6.36E-06
GO:0010876	lipid localization	7.11E-06
GO:0044710	single-organism metabolic process	1.47E-05
GO:0004866	endopeptidase inhibitor activity	2.03E-05
GO:0061135	endopeptidase regulator activity	2.19E-05
GO:0006508	proteolysis	2.56E-05
GO:0010951	negative regulation of endopeptidase activity	3.36E-05
GO:0051604	protein maturation	3.57E-05
GO:0016485|GO:0051605	protein processing	3.57E-05
GO:0052548	regulation of endopeptidase activity	4.90E-05
GO:0004857	enzyme inhibitor activity	8.22E-05
GO:0030414	peptidase inhibitor activity	8.22E-05
GO:0061134	peptidase regulator activity	8.87E-05
GO:0005579	membrane attack complex	9.72E-05
GO:0010466	negative regulation of peptidase activity	1.26E-04
GO:0008152	metabolic process	1.26E-04
GO:0051346	negative regulation of hydrolase activity	1.67E-04
GO:0052547	regulation of peptidase activity	1.67E-04
GO:0016787	hydrolase activity	1.76E-04
GO:0030168	**platelet activation**	2.71E-04
GO:0043086	negative regulation of catalytic activity	2.87E-04
GO:0044092	negative regulation of molecular function	3.92E-04
GO:0001944	**vasculature development**	7.73E-04

GO ACCESSION	GO Term	corrected p-value
GO:0048514	**blood vessel morphogenesis**	8.85E-04
GO:0001568	**blood vessel development**	0.00118
GO:0042060	**wound healing**	0.00226
GO:0016861	intramolecular oxidoreductase activity, interconverting aldoses and ketoses	0.00444
GO:0042157	lipoprotein metabolic process	0.00448
GO:0044765	single-organism transport	0.00553
GO:0005996	monosaccharide metabolic process	0.00803
GO:0006044	N-acetylglucosamine metabolic process	0.0104
GO:0005577	fibrinogen complex	0.0104
GO:0016860	intramolecular oxidoreductase activity	0.011
GO:0006810|GO:0015457|GO:0015460	transport	0.0111
GO:0051234	establishment of localization	0.0143
GO:0005215|GO:0005478	transporter activity	0.02478
GO:0019318	hexose metabolic process	0.0248
GO:1901605	alpha-amino acid metabolic process	0.0262
GO:0006006	glucose metabolic process	0.0317
GO:0016853	isomerase activity	0.0327
GO:0051179	localization	0.0329
GO:0060217	**hemangioblast cell differentiation**	0.0333
GO:0001570	**vasculogenesis**	0.0394
GO:0009611|GO:0002245	**response to wounding**	0.0394
GO:0017171	serine hydrolase activity	0.0394
GO:0008236	serine-type peptidase activity	0.0394
GO:0030234	enzyme regulator activity	0.0424
GO:0005975	carbohydrate metabolic process	0.0424
GO:0001525	**angiogenesis**	0.0446
GO:0016638	oxidoreductase activity, acting on the CH-NH2 group of donors	0.0461

Table 4.

Gene ontology (GO) term enrichment analysis using downregulated genes in *etv2*$^{ci32Gt-/-}$ embryos at 24 hpf stage.

GO ACCESSION	GO Term	corrected p-value
GO:0001568	blood vessel development	0.00512
GO:0001944	vasculature development	0.00697
GO:0048514	blood vessel morphogenesis	0.00697
GO:0004945	angiotensin type II receptor activity	0.0118
GO:0001595	angiotensin receptor activity	0.0118
GO:0038166	angiotensin-activated signaling pathway	0.0118
GO:0050900	leukocyte migration	0.028
GO:0005515|GO:0045308	protein binding	0.0287
GO:0004872|GO:0019041	receptor activity	0.0333
GO:0001653	peptide receptor activity	0.0333
GO:0008528	G-protein coupled peptide receptor activity	0.0333
GO:0004415	hyaluronoglucosaminidase activity	0.0346
GO:0004714	transmembrane receptor protein tyrosine kinase activity	0.0474
GO:0004553|GO:0016800	hydrolase activity, hydrolyzing O-glycosyl compounds	0.0474